Journal of Cleaner Production 272 (2020) 122875

Contents lists available at ScienceDirect

Journal of Cleaner Production

journal homepage: www.elsevier.com/locate/jclepro

Fall of oxidized while rise of reduced reactive nitrogen deposition in China

Lei Liu [a, *], Xiuying Zhang [b, **], Wen Xu [c], Xuejun Liu [c], Yan Zhang [d], Yi Li [e], Jing Wei [f], Xuehe Lu [b], Shanqian Wang [b], Wuting Zhang [b], Limin Zhao [b], Zhen Wang [b], Xiaodi Wu [b]

[a] College of Earth and Environmental Sciences, Lanzhou University, Lanzhou, 730000, China
[b] International Institute for Earth System Science, Nanjing University, Nanjing, 210023, China
[c] College of Resources and Environmental Sciences, National Academy of Agriculture Green Development, China Agricultural University, Beijing, 100193, China
[d] Shanghai Key Laboratory of Atmospheric Particle Pollution and Prevention (LAP3), Department of Environmental Science and Engineering, Fudan University, Shanghai, 200433, China
[e] SailBri Cooper Inc., Beaverto, OR, 97008, USA
[f] State Key Laboratory of Remote Sensing Science, College of Global Change and Earth System Science, Beijing Normal University, Beijing, China

ARTICLE INFO

Article history:
Received 12 March 2020
Received in revised form
18 May 2020
Accepted 14 June 2020
Available online 11 July 2020

Handling Editor: Bin Chen

Keywords:
Nitrogen deposition
Dry and wet deposition
Oxidized nitrogen
Reduced nitrogen
Satellite observation

ABSTRACT

China has the largest reactive nitrogen deposition worldwide. Understanding the change of nitrogen deposition and its socioeconomic drivers in China is crucial for the function and sustainability of regional and global ecosystems. Here we presented satellite-derived nitrogen deposition constrained with the national ground-based measurements over China. We found that oxidized nitrogen deposition peaked at 7.0 kg N ha^{-1} in 2012, then decreased to 6.2 kg N ha^{-1} in 2017. In contrast, reduced nitrogen deposition increased continuously, and reached 12.6 kg N ha^{-1} in 2017. The Chinese Clean Air Act is responsible for the reduction of oxidized nitrogen emissions, while there is no current effective control policy for ammonia emissions in place resulting in reduced nitrogen deposition reaching levels of approximately twice that of oxidized nitrogen in 2017. The ratio of reduced to oxidized nitrogen deposition decreased from 1.30 in 2008 to 1.08 in 2011, while this ratio began to increase from 1.08 in 2011 to 1.56 in 2017. This suggests reduced nitrogen deposition would become more important in the air quality and their ecological consequences in the future. The total nitrogen deposition in China was about 3–4 times that in the US and Europe. The policy of controlling nitrogen pollution is urgent, especially for reducing ammonia emissions, while ensuring the sustainable production of agriculture and maintaining food security.

1. Introduction

Global nitrogen (N) cycle throughout the earth system has been drastically altered by the introduction of reactive nitrogen (N_r, including oxidized and reduced N compounds) (Zhang et al., 2020) mainly from fossil fuel combustion and agriculture (Galloway et al., 2004). Atmospheric N_r deposition has implications to disturb the carbon cycle (Liu et al., 2005), causes biodiversity loss (Gao et al., 2018), increases acidification and eutrophication (Gao et al., 2019; Wei, 2020) and contaminates drinking water (Zhao et al., 2013). Quantifying N_r deposition is a prerequisite for assessing its consequences.

N_r deposition includes both reduced (NH_x) and oxidized N_r (NO_y) forms in wet (rainwater and snow) and dry processes (Dentener et al., 2006). China is the highest N_r producer worldwide with sharply increasing N_r emissions (Van Damme et al., 2018; Wang et al., 2012). Dry N_r deposition in China remains uncertain on large spatial scales resulting from the scarcity of available sites and long-term monitoring of both NO_y and NH_x (Liu et al., 2017c). Many previous works substantially underestimated total N_r deposition because only wet deposition was treated or just some parts of NO_y species (but not NH_x) were included (Xu et al., 2018). Moreover, the limited spatial representativeness of ground-based measurements contributes to the uncertainty, as N_r deposition is featured by

* Corresponding author.
** Corresponding author.
E-mail addresses: liuleigeo@lzu.edu.cn (L. Liu), zhangxy@nju.edu.cn (X. Zhang).

https://doi.org/10.1016/j.jclepro.2020.122875
0959-6526/

Abbreviation

ALPHA	Adapted Low-cost High Absorption
CTM	Chemistry transport model
DELTA	DEnuder for Long-Term Atmospheric
ECMWF	European Centre for Medium-Range Weather Forecasts
HNO_3	Nitric acid
IASI	Infrared Atmospheric Sounding Interferometer
MetOp	Meteorological Operational Satellite
N	Nitrogen
NH_3	Ammonia
NH_4^+	Ammonium
NH_x	Reduced reactive nitrogen deposition
NH_y	Reduced reactive nitrogen emission
NNDMN	National Nitrogen Deposition Monitoring Network
NO_2	Nitrogen dioxide
NO_3^-	Nitrate
NO_x	Oxidized reactive nitrogen emission
NO_y	Oxidized reactive nitrogen deposition
N_r	Reactive nitrogen
OMI	Ozone Monitoring Instrument
PM	Particular Matters

spatiotemporal heterogeneity. Satellite observations provide unique high-resolution datasets for estimating regional N_r deposition. A few studies used satellite-retrieved NO_2 data to derive the surface NO_x concentrations (Zhang et al., 2017b), dry NO_y deposition (Liu et al., 2017c) and wet NO_y deposition (Geddes and Martin, 2017; Liu et al., 2017a). NH_x deposition dominated the total N_r deposition (NO_y plus NH_x) based on measurements over China (Xu et al., 2018). Satellite NH_3 measurements have been proven to be powerful for monitoring the abundance of atmospheric NH_3 with numerous regional and global validations by ground-based measurements and aircraft measured NH_3 columns (Liu et al., 2017b; Van Damme et al., 2014).

Recent progress in the national N_r deposition measurements (National Nitrogen Deposition Monitoring Network, NNDMN) also made it possible to investigate and recognize the current status of both wet and dry N_r deposition over China. Here we used satellite-retrieved NO_2 and NH_3 columns to estimate N_r deposition over China constrained with the NNDMN measurements. Satellite-derived dry and wet N_r deposition in China was presented in this work, giving scientific background information for policy-makers to deal with China's N-enriched pollution challenge and reduce its ecological consequences. This is extremely important considering the background that China's policies focus on green development and increasingly stricter environmental protection.

2. Materials and methods

2.1. Observational data

All observational data on N_r deposition and concentrations used in this study originated from the NNDMN over China, comprising background, rural and urban types (Xu et al., 2015). It covers six geo-climatic and social-economic regions in China, including the Tibetan Plateau, Southwestern China, Northeastern China, Northwestern China, Southeastern China and Northern China. N_r species monitored in the NNDMN included oxidized (gaseous NO_2, HNO_3, particulate NO_3^- and wet NO_3^-) and reduced N_r (gaseous NH_3, particulate NH_4^+ and wet NH_4^+). Dry N_r deposition is not a direct measurement conducted by the NNDMN due to the requirements for sophisticated methods and instrumentation (Flechard et al., 2011b; Sutton et al., 2001). Instead, the surface gaseous and particulate N_r concentrations were measured.

Surface gaseous HNO_3, NO_2 and NH_3 concentrations, and particulate NH_4^+ and NO_3^- in the particulate matter (the diameter is 4–5 μm) were monitored by both passive and active samplers. Gaseous NH_3, HNO_3, and particles were monitored by DEnuder for Long-Term Atmospheric (DELTA) active sampling systems. If the DELTA systems cannot work due to electricity constraints, the Adapted Low-cost High Absorption (ALPHA) passive samplers were used to measure NH_3 concentrations (Zhang et al., 2010), while NH_4^+ and NO_3^- in particular matters (PM) were measured by particulate samplers. The two methods used by the DELTA and ALPHA systems to measure surface NH_3 concentrations were consistent (Xu et al., 2015). NO_2 concentrations were measured by Gradko diffusion tubes (Skiba et al., 2006) at all sampling sites. Wet N_r deposition (rainwater and snow) was monitored by precipitation gauges, including a glass bottle and stainless steel funnel. The monitoring results of gaseous, particulate, wet N_r concentrations and deposition in the NNDMN have been published (Xu et al., 2015, 2019). This study used the ground-based measured gaseous NH_3 and NO_2 concentrations in the NNDMN to verify the estimates. Measured wet NH_4^+ and NO_3^- deposition during 2010–2012 were used to establish the mixed-effects models, while wet deposition during 2013–2014 was used to validate the satellite-based estimates.

2.2. Satellite data

We applied satellite NO_2 column products by Ozone Monitoring Instrument (OMI) onboard NASA's EOS Aura to estimate the oxidized N_r deposition. The Aura overpass time crossing the equator was 13:00–14:00, providing global NO_2 retrievals (Boersma et al., 2007). OMI NO_2 retrieval used the reflectance spectra from 405 to 465 nm, and considered smooth spectral features resulting from Mie scattering, Rayleigh and surface albedo (Lamsal et al., 2015). Updates of using gas profiles and column temperature from European Centre for Medium-Range Weather Forecasts (ECMWF) for air mass factor were introduced for improving the temperature sensitivity to NO_2 spectrum (Boersma et al., 2011). The DOMINO v2.0 product was used at 0.125° grids on a monthly scale during 2005–2017 (Boersma et al., 2011), which have been widely used in many scientific applications such as estimating the NO_x emissions, identifying the hotspots of NO_x and environmental related studies (Lamsal et al., 2010; Schaub et al., 2006).

We also used the satellite NH_3 column products from Infrared Atmospheric Sounding Interferometer (IASI) onboard the meteorological platforms of MetOp-A, crossing the equator at 09:30 and 21:30. IASI used the infrared radiation in the spectra between 645 and 2769 cm^{-1} (Van Damme et al., 2018). We used satellite retrievals during 2008–2017 at 9:30 since they are more sensitive to NH_3 with high thermal contrast (http://iasi.aeris-data.fr/NH3/). IASI NH_3 column products were derived by Artificial Neural Network algorithms with several updates (Van Damme et al., 2017), considering the impact of temperature, pressure and humidity vertical profiles. The monthly NH_3 columns were averaged by daily retrievals at 0.25° grids (Liu et al., 2019). IASI NH_3 retrievals have been applied in numerous scientific works such as estimating the NH_3 emissions (Dammers et al., 2019), identifying the NH_3 hotspots (Van Damme et al., 2018), exploring the trends of atmospheric NH_3 and environmental related studies (Zhang et al., 2017a).

2.3. Estimating dry and wet N_r deposition

This study evaluated N_r species of gases, particles and precipitation. Total N_r deposition was derived by summing gaseous and particulate dry N_r deposition, and wet N_r deposition. Dry deposition can be expressed by the following equation (Flechard et al., 2011a):

$$F = G_S V_d \quad (1)$$

where G_S is the surface N_r concentrations; V_d represents the deposition velocity of N_r species, defined as follows (Sportisse, 2007; Wesely and Hicks, 1977):

$$V_d = \frac{1}{R_a + R_b + R_c} + V_g \quad (2)$$

where R_a, R_b, and R_c represent aerodynamic resistance, penetration resistance and canopy resistance. For particles (NO_3^-, NH_4^+), canopy resistance is often assumed to be zero ($R_c = 0$) because particles are believed to usually adhere to the surface on contact. V_g is the gravitational settling velocity determined by particle size and density, and cannot be neglected for particles during the deposition process.

Surface NO_2 and NH_3 concentrations were estimated by combining their vertical profiles and satellite-retrieved columns. Satellite-derived surface NO_2 or NH_3 concentrations are calculated as (Graaf et al., 2018; Liu et al., 2019):

$$S_G = S_{trop}\frac{\rho(h_G)}{F(h_{trop})} \quad (3)$$

where S_{trop} represents the NO_2 or NH_3 columns from satellite; $\rho(h_G)$ is the surface NO_2 or NH_3 concentrations at the height of h_G and $F(h_{trop})$ is the NO_2 or NH_3 columns from a chemistry transport model (CTM, see the Supporting Information).

Surface particulate NO_3^- and gaseous HNO_3 concentrations were calculated using satellite-derived surface NO_2 estimates and the relationship between surface NO_2 and NO_3^-, while surface particulate NH_4^+ concentrations were estimated by satellite-derived surface NH_3 concentrations and the relationship of surface NH_3 and NH_4^+. The correlation between the surface NO_2 and NO_3^- concentrations was 0.76 from NNDMN; the correlation between the surface NO_2 and HNO_3 concentrations was 0.88; the correlation between the surface NH_3 and NH_4^+ concentrations was 0.86 (Fig. S2).

Mixed-effects models (Hedeker, 2010; Stram, 1996) were used to estimate wet N_r depositions based on satellite observations and meteorological variables. Mixed effect models, also known as hierarchical models, describe the relationship between dependent variables (such as wet deposition) and independent variables (such as N compounds in the atmosphere and meteorological variables), and the coefficients can vary according to one or more grouped variables (Stram, 1996; Yap and Hashim, 2013). Mixed-effect models include two parts: random effect and fixed effect. Fixed effect items are usually part of traditional linear regression, while random effects are associated with individual randomly selected experimental factors (such as different land-use types) (Hedeker, 2010; Morrell, 1998). For the wet NH_4^+ deposition, the following equations were used:

$$NH_4^+N_{ijk} = \left(\alpha_{fix} + \alpha_i + \alpha_k\right) + (\beta_i + \gamma_k)S_{ij} + \varepsilon_{ij} \quad (4)$$

where

$$S_{ij} = P_{ij}(NH_3)_{ij}$$

$NH_4^+N_{ijk}$ is measured wet NH_4^+ deposition from the NNDMN in month i, site j, and land-use type k, where 0, 1 and 2 represent urban, farmland and other land use types, respectively; $(NH_3)_{ij}$ is IASI NH_3 columns in month i and site j; P_{ij} represents precipitation amounts in month i and site j; S_{ij} represents an indicator of the combined effect of NH_3 and precipitation; α_{fix} is the fixed intercept for all months and sites representing the average effects, while α_i and α_k represent random intercepts by month and land-use. β_i is random slopes in month i and site j representing effects of S_{ij} on $NH_4^+N_{ij}$ for different months, while γ_k (k=[0, 1, 2]) represents random slopes by land-use types. ε_{ij} represents the residuals.

NO_2 contributes to wet NO_3^- deposition in precipitation through indirect way through reacting with O_3 or OH radical to form NO_3^- or N_2O_5 (Mentel et al., 1996; Miyazaki et al., 2012). Wet NO_3^- deposition was mainly from the scavenging of particulate NO_3^- and gaseous HNO_3. NO_2 can be an indicator of oxidized N_r components, and significantly linked with HNO_3 and NO_3^- within the atmospheric boundary layer (Liu et al., 2017a). Estimation of wet NO_3^- depositions can achieve high predictive accuracy including the seasonal random intercepts, as the following equations (Liu et al., 2017a):

$$NO_3^-N_{ij} = \left(\alpha_{fix} + \alpha_i\right) + \beta_{fix}S_{ij} + \varepsilon_{ij} \quad (5)$$

where

$$S_{ij} = P_{ij}(NO_2)_{ij}$$

$NO_3^-N_{ij}$ is the measured wet NO_3^- deposition from the NNDMN in month i and site j; $(NO_2)_{ij}$ is OMI NO_2 columns in month i and site j; P_{ij} indicates precipitation amounts in month i at site j; S_{ij} represents an indicator of the combined effects of N compounds and precipitation; α_{fix} and α_i represent the fixed and random intercepts; β_{fix} indicates the fixed slopes. We used the measured wet NH_4^+ and NO_3^- deposition during 2010–2012 to establish mixed-effects models, while measured wet deposition during 2013–2014 was used to validate the satellite estimates. Please refer to Table S2 and Table S3 for each parameter of mixed-effects models.

3. Results

3.1. Validation of satellite-derived estimates

We spatially expand ground measurements of N_r deposition at the NNDMN monitoring sites to national scale through integrating satellite observations and models. Dry N_r deposition is not a direct measurement conducted by the NNDMN, in which surface N_r concentrations were measured and then multiplied by modeled V_d. Satellite-derived surface NO_2 and NH_3 estimates were contrasted with the ground-based concentrations at the NNDMN sites (Fig. 1). Satellite-derived estimates explained the variability of surface NO_2 concentrations (slope = 1.03, intercept = −1.08 and R = 0.87). The average of estimated surface NO_2 concentrations over monitoring sites in 2012 were 6.80 μg N m^{-3}, slightly higher than measurements (5.97). Measured surface NH_3 concentrations at the NNDMN sites were also contrasted with the satellite estimates (slope = 0.62 and R = 0.84). The average of estimated surface NH_3 concentrations over monitoring sites in 2012 was 5.94 μg m^{-3}, similar to that of ground-based measurements (6.65). However, several sites over Yunnan showed relatively larger absolute errors for NO_2, and

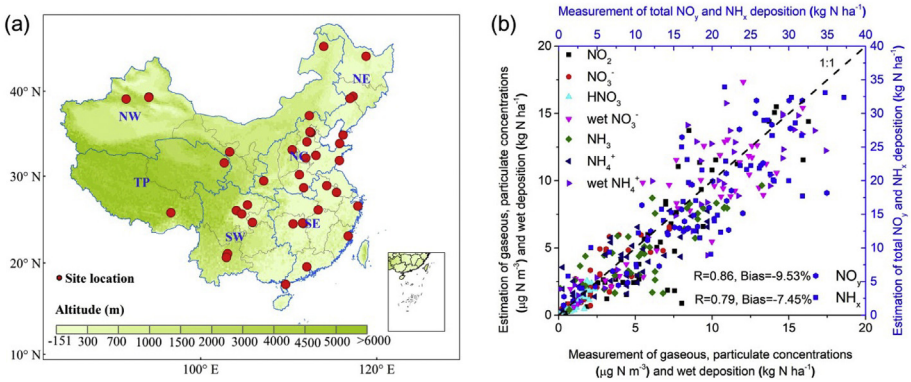

Fig. 1. Geographical locations of the NNDMN sites (a), and comparison of satellite retrieved N_r deposition and concentrations with measurements at the NNDMN sites (b). Six geographical regions are the Tibetan Plateau (TP), Southwestern China (SW), Northeastern China (NE), Northwestern China (NW), Southeastern China (SE) and Northern China (NC). Here R in the figure means correlation coefficient. We also added the residual plots for Eqs. (4) and (5) as Fig. S6 in the Supporting Information.

several sites in Gansu, eastern Sichuan and Chongqing showed relatively larger absolute errors for NH_3 (Fig. S3), which may be linked with limited spatial representatives of monitoring sites as well as the uncertainty of satellite estimates. Similarly, we also compared wet N_r deposition with the monitoring results in the NNDMN. Overall, the satellite-based estimates can capture the general spatial distributions of wet NO_3^- deposition (slope = 0.86, R = 0.86) and wet NH_4^+ deposition (slope = 0.74, R = 0.81). The satellite-based estimates of N_r deposition show good agreement with measurements for NO_y (R = 0.86 and Bias = −9.53%) and NH_x deposition (R = 0.79 and Bias = −7.45%).

3.2. Spatial variations of N_r deposition in China

Total N_r deposition over China in 2012 was estimated at 18.21 kg N ha^{-1} (Fig. 2a), in which wet and dry N_r deposition accounted for 57% and 43%. Atmospheric N_r deposition varied substantially, with lower values over Western regions and higher values over Eastern China. Highest total N_r deposition was found in Northern China (NC), a region with centralized management of agricultural land and which is economically developed, at 38.33 kg N ha^{-1} for the year 2012; the lowest N_r deposition appeared over the Tibet Plateau (TP), at 5.01 kg N ha^{-1}. Spatial pattern of N_r deposition correlates with large gradients in socio-economic indicators (R^2 = 0.85 for deposition vs. GDP; R^2 = 0.83 for deposition vs. population in Fig. S4).

The percentage of dry to total N_r deposition was 43% on average in 2012, which was slightly lower than that (50%) measured by the NNDMN. The ratio of dry to total N_r deposition shows different spatial patterns in six regions of China. In NC, most areas had wet N_r deposition below 30 kg N ha^{-1}, while vast area had dry N_r deposition above 30 kg N ha^{-1}. Instead, over southern coastal provinces we found wet N_r deposition dominated the total N_r with values higher than 20 kg N ha^{-1}, while dry N_r deposition was below 20 kg N ha^{-1} except for some areas over Guangdong province. The NC region had the largest dry/total ratio (~50% on average), while the southern China (including SE and SW) had the smallest dry/total ratio (approximately 37% on average), indicating that this region is dominated by wet deposition (Fig. 2), as precipitation events are more frequent.

3.3. Fractional N_r species for N_r deposition

Regarding oxidized and reduced N_r, NO_y and NH_x deposition accounted for 34% and 66%. NO_y and NH_x deposition exhibited markedly different spatial patterns. NO_y deposition mainly occurred in urban areas with several hotspots found in the densely populated metropolitan areas such as for instance Beijing-Tianjin or Yangtze Delta regions. These hotspots generally show NO_y deposition rates of 20–30 kg N ha^{-1}, while rates below 10 kg N ha^{-1} were found over other Eastern and Middle regions, and Western China, respectively. In contrast, NH_x deposition mainly occurred in intensive agricultural regions, such as the NC, Sichuan Basin, and low-middle reaches of Yangtze River Basin, which represent main food baskets for the Chinese population (Huang et al., 2012). As a key difference, to the scatted distribution of NO_y deposition, the hotspots of NH_x deposition are more widely distributed. Deposition rates of NH_x greater than 30 kg N ha^{-1} were commonly found over agricultural regions for instance the NC.

In total, dry NO_y, wet NO_3^-, dry NH_x and wet NH_4^+ deposition accounted for about 13%, 25%, 30% and 32% for the total N_r deposition, respectively (Fig. 3 c). For different components in oxidized N_r deposition, wet NO_3^- deposition contributed about 67% to the total oxidized N_r deposition, followed by dry HNO_3 (20%), NO_2 (7%) and particulate NO_3^- (6%) in China (Fig. 3). Dry HNO_3 deposition was the second (20%) primary contributor to oxidized N_r deposition, which is mainly due to its high deposition velocity. The average deposition velocity of HNO_3 over China is 1.39 cm s^{-1}, much higher than the deposition velocity of particulate NO_3^- and gaseous NO_2 (below 0.20 cm s^{-1}). Regarding different components of reduced N_r deposition in China, wet NH_4^+ deposition dominated the total reduced N_r deposition (52%), while the dry NH_3 and particulate NH_4^+ contribute about 33% and 15% of total reduced N_r deposition, respectively (Fig. 3 b).

3.4. Trends of N_r deposition over China

Satellite-derived dry and wet oxidized N_r deposition in China during 2005–2017 is shown in Fig. 4a. Dry NO_y deposition increased by 0.25 kg N ha^{-1} per year between 2005 and 2011, while it decreased by −0.23 kg N ha^{-1} per year between 2011 and 2016. For wet NO_3^- deposition, a slight increase (0.08 kg N ha^{-1} per year) occurred between 2005 and 2010; however, there was a drop (approximately −0.14) for the year 2011 with the lowest precipitation since 2005 (approximately 557 mm). In contrast with the obvious decrease in dry NO_y deposition, wet NO_3^- deposition became stable after 2011 with small fluctuations. The decline in oxidized N_r deposition during 2011–2017 (−0.24 kg N ha^{-1} per year) was mainly driven by the significant decrease of dry NO_y deposition. These reductions of oxidized N_r deposition are mainly

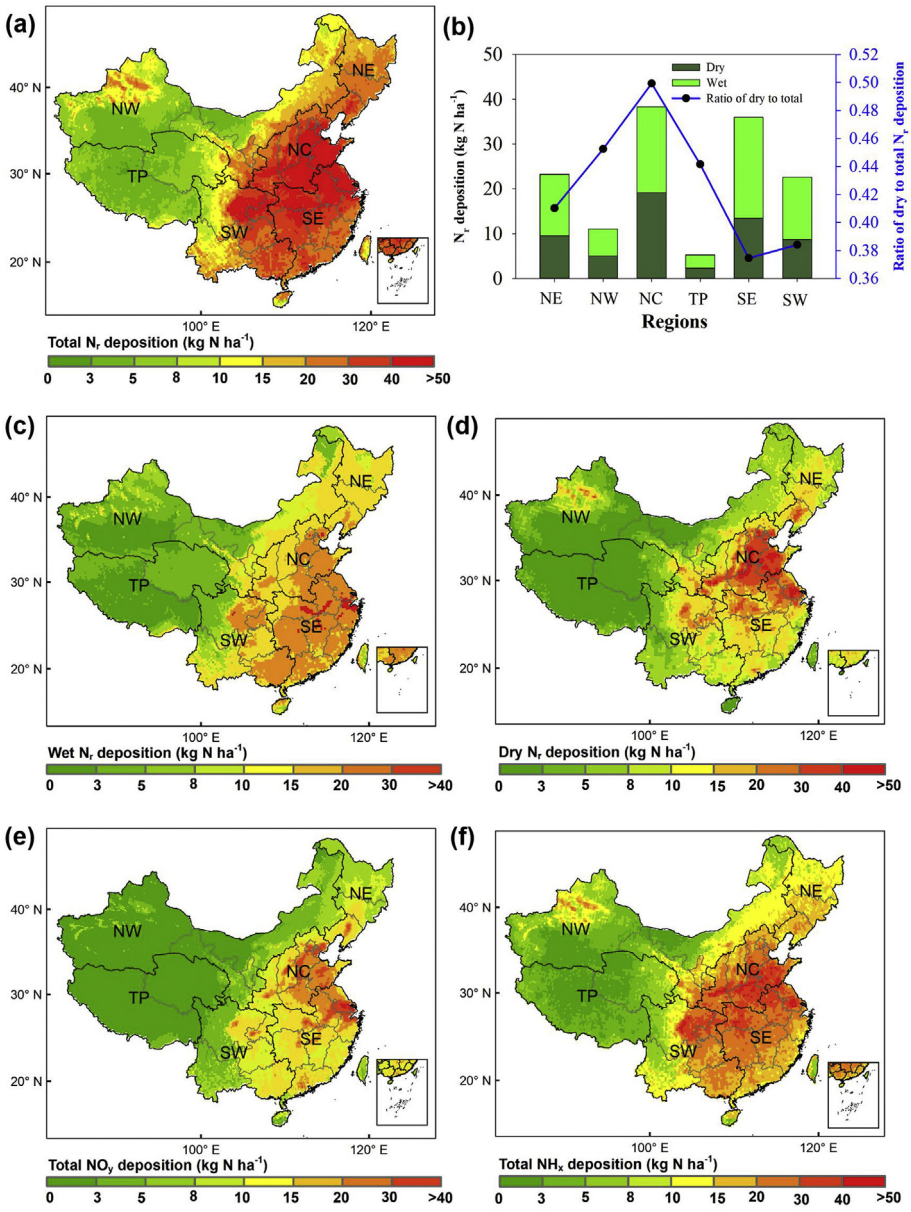

Fig. 2. Atmospheric N_r deposition in China. (a), (c), (d), (e) and (f) are spatial distribution of atmospheric total, wet, dry, NO_y and NH_x deposition in 2012; (b) is descriptive statics of satellite-retrieved N_r deposition and dry/total ratio in the six geographical regions.

due to the effectiveness of the strong control policy on NO_x emissions. Correspondingly, there was an obvious increase in the ratio of dry to oxidized N_r deposition during 2005–2011 (0.01 y^{-1}) and a decline during 2011–2017 (−0.01 y^{-1}).

Satellite-derived reduced N_r deposition over China during 2008–2017 is shown in Fig. 4b. An increase of 0.21 kg N ha^{-1} per year for dry NH_x and 0.09 for wet NH_4^+ occurred during 2008–2017. In total, reduced N_r deposition increased by 0.30 kg N ha^{-1} per year, which was associated with the increased NH_3 emissions as well as the lack of control regulations.

Total N_r deposition (reduced plus oxidized) in China increased by 0.28 kg N ha^{-1} per year between 2008 and 2017. The ratio of NH_x to NO_y deposition decreased from 1.30 in 2008 to 1.08 in 2011, while this ratio began to increase from 1.08 in 2011 to 1.56 in 2017 (0.09 y^{-1}, $p = 0.00$), which can be attributed to the decline in NO_y deposition after 2011 and the continued increase in NH_x deposition. Thus, NH_x deposition dominates the total N_r deposition and will become more important for total N_r. The contributions of dry to total N_r deposition varied with small fluctuations (41–44% on average over China) during 2008–2017, implying its importance of dry N_r deposition and its important effects on terrestrial ecosystems.

3.5. Comparison with other studies

To estimate N_r deposition at large scales, previous studies were usually based on applying the arithmetic average methods to monitoring data, geostatistical methods (e.g., Kriging interpolation of monitoring data) or CTMs (e.g., EMEP, GEOS-Chem or MOZART) (Table S5 and Fig. 5a). The resulting estimates of total N_r deposition in China by this work (18.19 kg N ha^{-1}) were reasonably lower compared to the national NNDMN measurements (36.5 kg N ha^{-1}) using arithmetic average methods, due to the influence of monitoring sites mainly being located in Eastern China, which have

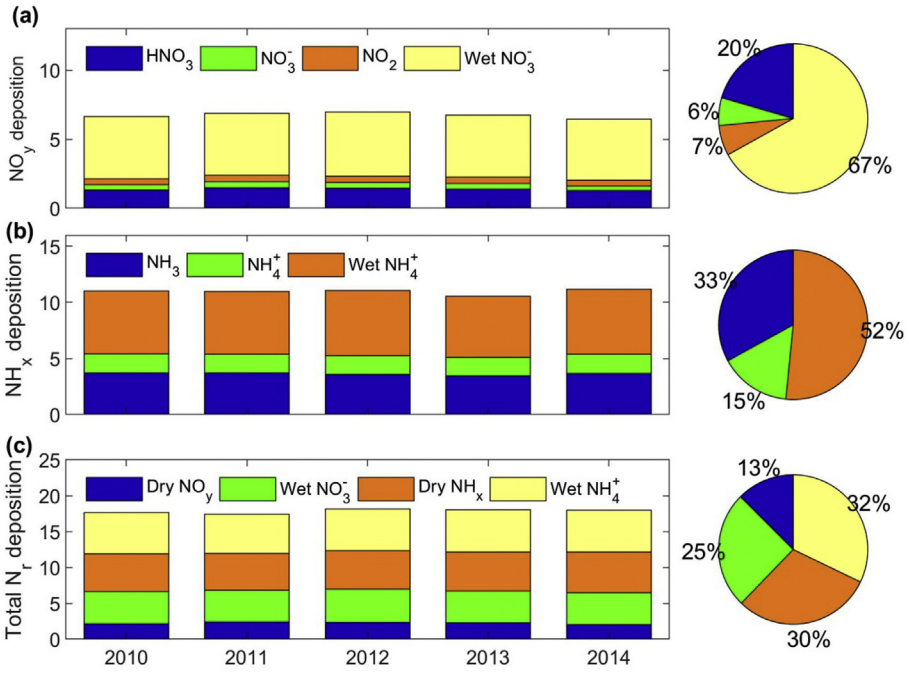

Fig. 3. Fractional N_r species to N_r deposition. (a) fractional gaseous HNO_3, NO_2, particulate NO_3^- and wet NO_3^- to total oxidized N_r; (b) fractional gaseous NH_3, particulate NH_4^+ and wet NH_4^+ deposition to total reduced N_r; (c) fractional dry NO_y, wet NO_3^-, dry NH_x and wet NH_4^+ to the total N_r.

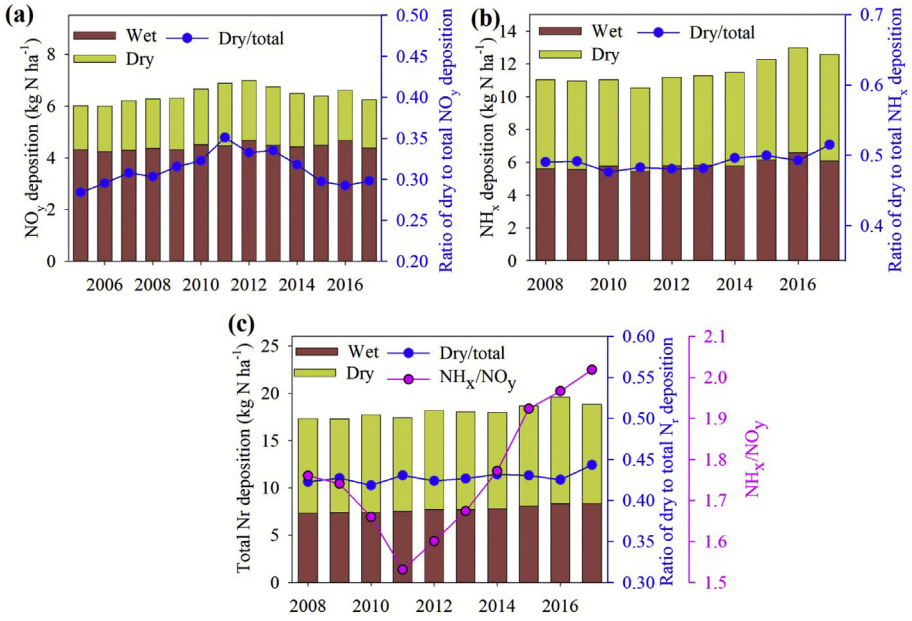

Fig. 4. Time series of satellite-derived wet and dry N_r deposition over China. (a), (b) and (c) indicate NO_y, NH_x and total N_r respectively.

considerably higher N_r deposition. Satellite-based estimates in this study were higher than Liu et al. (12.80) and Zhu et al. (13.69), since their estimates did not include the dry N_r deposition (Liu et al., 2016; Zhu et al., 2015), which we explicitly include in our estimates. Moreover, our estimates were comparable to the results from CTMs by Zhao et al. (17.36) and Yu et al. (19.60) (Yu et al., 2019; Zhao et al., 2017). The estimates in this study were within the ranges of estimates by previous studies, and may provide a more realistic spatial picture of N_r deposition in China compared with the NNDMN sites.

We compared N_r deposition in China with that in the US and Europe in Fig. 5. Atmospheric N_r deposition in China was more double than that in the US and Europe due to more intensive NH_3 and NO_x emission. In 2010, NH_3 emission in China (15.05 Tg N y^{-1}) was estimated approximately 3.67 and 3.38 times than that in the US (4.13) and Europe (4.45), respectively; NO_x emission in China (8.43 Tg N y^{-1}) was estimated approximately 2.01 and 3.57 times than that in the US (4.20 Tg N y^{-1}) and Europe (2.36 Tg N y^{-1}), respectively, based on the global EDGAR emissions. In total, the sum of NH_3 and NO_x emission in China (23.48 Tg N y^{-1}) was

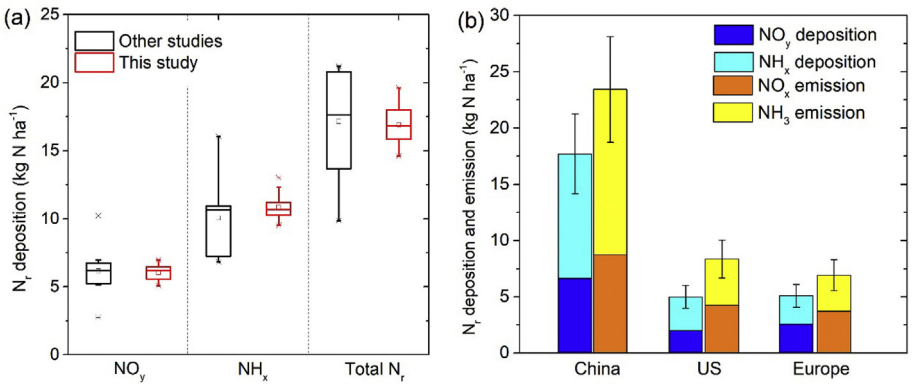

Fig. 5. Comparison of atmospheric N_r deposition (kg N ha^{-1}) between China and other countries. (a) atmospheric N_r deposition (kg N ha^{-1}) in China in previous studies and this study (Table S5); (b) comparison of atmospheric N_r deposition and N_r emission (kg N ha^{-1}) in China, US and Europe. N_r deposition in the US was gained from a recent study by Zhang et al. (Zhang et al., 2018); N_r deposition in Europe was gained from Tan et al. (Tan et al., 2018).

approximately 2.82 and 3.45 times than that in the US (8.33) and Europe (6.81). Total N_r deposition in China in the 2010s was similar to values of N_r deposition in Europe and the US in the 1980s with peak atmospheric N_r deposition (Larssen et al., 2006).

4. Discussion

Estimating high-resolution N_r deposition over China is crucial to evaluate future policy implications regarding mitigation options (Liu et al., 2013; Sutton et al., 2013). Our work presents the comprehensive estimates of N_r deposition for China by integrating satellite observations, ground-based measurements and models at a high spatial resolution over a long time period. We conducted a thorough evaluation of wet and dry N_r, which is essential for gaining an overall insight into the current status of China's N_r deposition, considering the background that most previous works focused on wet deposition and the measurements of dry N_r deposition are still very lacking. In the field of using satellite retrievals to estimate N_r deposition, some progress has been made, but there are still some problems to be solved. First, satellite NO_2 and NH_3 retrievals used in this work are instantaneous observations, and using multi-phase satellite data to estimate N_r deposition is worth further study in the future. New generation of high-resolution sensors of TEMPO (North America), Sentinel (Europe) and GEMS (Asia) can improve the time resolution of satellite observations, and possibly reduce the missing data caused by clouds, which will undoubtedly improve the accuracy of estimating N_r deposition. Second, with the development of space technology, more and more N_r components can be detected. For example, atmospheric HNO_3 can be detected by the IASI sensor, and relevant research has been devoted to the development of more reliable satellite HNO_3 products. Using more satellite data of N_r components to estimate regional N_r deposition can reduce the uncertainties of other N_r (such as HNO_3, NO_3^-) deposition.

On the national scale, the dry/total ratio was higher than 40% during 2008–2017, suggesting the importance of dry N_r deposition. Due to incomplete measurements of dry deposition, previous studies often underestimated its contributions to total N_r deposition (Liu et al., 2011). For example, NH_3, HNO_3, particulate NH_4^+ and NO_3^- were not included in estimating dry deposition (Lü and Tian, 2007), which caused large underestimation of total N_r deposition over China. Moreover, previous research on N_r deposition was mainly on wet or bulk deposition over China or on NO_y deposition (but not including NH_x deposition). Dry N_r deposition in NC can be approximately 50% of total N_r deposition in this study, which was very close to the estimates (28–67%, on average ~50%) at ten sites (Pan et al., 2012).

The continuous declines in NO_y deposition occurred since 2011, reflecting that the policy established to control NO_x emissions by the Chinese government has achieved considerable effectiveness. By 2015, a reduction of NO_x emissions by −10% (compared to 2010 levels) had been achieved, as identified as an essential goal to evaluate the performance of local governments (Foy et al., 2016). NO_x emission control technologies had been installed in large combustion plants and other boilers, and upgraded emission standards of road transport vehicles, alongside gasoline and diesel fuel quality standards had been implemented rapidly. As a result, total NO_x emissions have been reduced and our results demonstrate the effect of these policy interventions on the NO_y deposition, with approximately a −11% reduction in the period from 2012 to 2017.

However, NH_x deposition has increased continuously since 2008 due to the lack of control policies on NH_3 emission from agriculture, in the context of substantial pressures to maintain food security, given that China feeds 22% of world population with only 9% of global croplands (Piao et al., 2010). Our estimates of reduced N_r deposition were consistent with temporal variations of NH_3 emissions by a recent study (Zhang et al., 2017a) as well as the satellite retrievals both from IASI and AIRS (Liu et al., 2019; Warner et al., 2017). Moreover, agricultural non-point source pollution has to date mainly been considered as relevant for water pollution, while its contribution to air pollution has been widely neglected in China (Wei et al., 2019a, 2019b). Many currently applied measures, such as air drying treatment of manure, in fact, accelerate NH_3 emission as an unintended consequence of the original intention to reduce N_r loss to water bodies (Gu et al., 2015).

Currently, atmospheric N_r deposition in China was more double than that in the US and Europe. The big difference of N_r deposition level between China, the US and Europe was associated with the population, technologies and management standards. China's population of 1.4 billion people in 2016 was 4.3 times than the US (0.3 billion) and 1.75 times than Europe (0.8 billion). The pressure from the large population and increased per capita consumption of agricultural products in China promoted more agricultural production enormously related to synthetic N_r fertilizer production and application (Diamond, 2005; Geddes et al., 2016). Many Chinese economies remain obsolete and inefficient, and the efficiency of industrial energy is approximately half of that compared with developed countries (Deng et al., 2008; Diamond, 2005).

In terms of the policy, the implementation of regulations and laws on controlling N_r emissions in China was generally much later than the US and Europe. Europe's peak N_r production appeared in the 1980s related to agricultural over-production. Since 1990, effective policies were implemented over Europe, and NO_x and NH_3 emissions were reduced by −31% and −29% from 1990 to 2009 (Tørseth et al., 2012). The success of the control policies by the US government on NO_x emissions between 1990 and 2010 also made NO_x emissions decrease by approximately −41%, while NH_3 emissions raised by 11% during 1990–2010 (Li et al., 2016). Rising importance of reduced N_r deposition occurred in China due to the decrease in oxidized N_r deposition since 2011 and the increase in reduced N_r deposition. China needs to control the oxidized and reduced N_r at the same time in a balanced way to slow down the increase of N_r deposition and its negative impacts on the environment. NH_3 contributes to the formation of secondary inorganic aerosols that affect environmental and human health and reduce visibility (Hasheminassab et al., 2014; Kloog et al., 2015). The importance of agricultural NH_3 pollution has been now recognized by China's central government in the 13th Five-Year Plan (2016–2020), and the "Zero Increase Action Plan" (ZIAP) was implemented to maintain and further reduce mineral fertilizer use in China (Liu et al., 2015).

To meet human health security goals and improve air quality and the ecosystems, future policies should focus on controlling NH_3 emissions as a priority (Gu et al., 2014). Using N_r to promote agricultural production while protecting the environment simultaneously is a great challenge for China. Spatiotemporal variations of N_r deposition were strongly heterogeneous, suggesting the urgency to implement comprehensive pollution control strategies to reduce risks linked to N_r deposition. Recent studies reveal high potentials in mitigating NH_3 losses from both croplands and livestock sectors (Li et al., 2017b), and new urease inhibitors reduce NH_3 volatilization and improve N use efficiency of Maize in North China Plain (Li et al., 2017a), which, in the future, need to be further implemented and verified in other regions to confirm the effectiveness for mitigating NH_3 losses.

5. Conclusions

Human activities, including the agricultural production and fossil fuels combustion, have greatly increased emissions of N_r to the atmosphere. This article provides the satellite-based, national assessment of wet and dry N_r deposition, constrained with national measurements (NNDMN). We demonstrated oxidized and reduced N_r deposition in China and highlight the key drivers for the recent trends observed. Increasing N_r emissions in China have resulted in substantially higher N_r deposition than in the US and Europe, highlighting the urgent need for China to tackle the increasing N_r deposition levels to reduce adverse effects on human and environmental health. Fortunately, we observe continuous declines in oxidized N_r deposition since 2012, which reflects that the policy established to control oxidized N_r emission by the Chinese government has been effective. However, reduced N_r deposition in China has increased continuously since 2008 due to the lack of effective control policies on NH_3 emissions. Increasing reduced N_r deposition in China suggests that it is key to address reduced N_r to mitigate total N_r deposition, and it will be increasingly important in the future with a further increase in the relative contribution of reduced N_r. Reducing the risks linked to total N_r emission and deposition with enforced control strategies is crucial, paying particular attention to pollution swapping and unintended consequences of single-compartment focused policy measures.

CRediT authorship contribution statement

Lei Liu: Conceptualization, Methodology, Writing - original draft. **Xiuying Zhang:** Conceptualization, Methodology, Writing - original draft. **Wen Xu:** Validation, Formal analysis, Visualization, Investigation. **Xuejun Liu:** Validation, Formal analysis, Visualization, Investigation. **Yan Zhang:** Validation, Formal analysis, Visualization, Investigation. **Yi Li:** Writing - review & editing. **Jing Wei:** Writing - review & editing. **Xuehe Lu:** Writing - review & editing. **Shanqian Wang:** Validation, Formal analysis, Visualization, Investigation. **Wuting Zhang:** Validation, Formal analysis, Visualization, Investigation. **Limin Zhao:** Validation, Formal analysis, Visualization, Investigation. **Zhen Wang:** Validation, Formal analysis, Visualization, Investigation. **Xiaodi Wu:** Validation, Formal analysis, Visualization, Investigation.

Declaration of competing interest

The authors declare that they have no known competing financial interests or personal relationships that could have appeared to influence the work reported in this paper.

Acknowledgements

This work is supported by National Natural Science Foundation of China (Nos. 41471343, 41425007 and 41101315) as well as Chinese National Programs on Heavy Air Pollution Mechanisms and Enhanced Prevention Measures. We thank Dr. Baojing Gu at Zhejiang University and Dr. Stefan Reis at Centre for Ecology & Hydrology for helpful comments and discussions.

Appendix A. Supplementary data

Supplementary data to this article can be found online at https://doi.org/10.1016/j.jclepro.2020.122875.

References

Boersma, K., Eskes, H., Veefkind, J.P., Brinksma, E., Van Der A, R., Sneep, M., Van Den Oord, G., Levelt, P., Stammes, P., Gleason, J., 2007. Near-real time retrieval of tropospheric NO_2 from OMI. Atmos. Chem. Phys. 7, 2103–2118.

Boersma, K.F., Eskes, H.J., Dirksen, R.J., van der A, R.J., Veefkind, J.P., Stammes, P., Huijnen, V., Kleipool, Q.L., Sneep, M., Claas, J., Leitão, J., Richter, A., Zhou, Y., Brunner, D., 2011. An improved tropospheric NO_2 column retrieval algorithm for the Ozone Monitoring Instrument. Atmos. Meas. Tech. 4, 1905–1928.

Dammers, E., McLinden, C.A., Griffin, D., Shephard, M.W., Van Der Graaf, S., Lutsch, E., Schaap, M., Gainairu-Matz, Y., Fioletov, V., Van Damme, M., Whitburn, S., Clarisse, L., Cady-Pereira, K., Clerbaux, C., Coheur, P.F., Erisman, J.W., 2019. NH_3 emissions from large point sources derived from CrIS and IASI satellite observations. Atmos. Chem. Phys. 19, 12261–12293.

Deng, X., Huang, J., Rozelle, S., Uchida, E., 2008. Growth, population and industrialization, and urban land expansion of China. J. Urban Econ. 63, 96–115.

Dentener, F., Drevet, J., Lamarque, J., Bey, I., Eickhout, B., Fiore, A., Hauglustaine, D., Horowitz, L., Krol, M., Kulshrestha, U., 2006. Nitrogen and sulfur deposition on regional and global scales: a multimodel evaluation. Global Biogeochem. Cycles 20.

Diamond, J., 2005. China's Environment in a Globalizing World: how China and the rest of the world affect each other. World Environ. 435, 1179–1186.

Flechard, C., Nemitz, E., Smith, R., Fowler, D., Vermeulen, A., Bleeker, A., Erisman, J., Simpson, D., Zhang, L., Tang, Y., 2011a. Dry deposition of reactive nitrogen to European ecosystems: a comparison of inferential models across the NitroEurope network. Atmos. Chem. Phys. 11, 2703–2728.

Flechard, C.R., Nemitz, E., Smith, R.I., Fowler, D., Vermeulen, A.T., Bleeker, A., Erisman, J.W., Simpson, D., Zhang, L., Tang, Y.S., 2011b. Dry deposition of reactive nitrogen to European ecosystems: a comparison of inferential models across the NitroEurope network. Atmos. Chem. Phys. 2011, 2703–2728.

Foy, B.D., Lu, Z., Streets, D.G., 2016. Satellite NO_2 retrievals suggest China has exceeded its NO_x reduction goals from the twelfth Five-Year Plan. Sci. Rep. 6, 35912.

Galloway, J.N., Dentener, F.J., Capone, D.G., Boyer, E.W., Howarth, R.W., Seitzinger, S.P., Asner, G.P., Cleveland, C., Green, P., Holland, E., 2004. Nitrogen cycles: past, present, and future. Biogeochemistry 70, 153–226.

Gao, Y., Jia, Y., Yu, G., He, N., Zhang, L., Zhu, B., Wang, Y., 2019. Anthropogenic

reactive nitrogen deposition and associated nutrient limitation effect on gross primary productivity in inland water of China. J. Clean. Prod. 208, 530–540.
Gao, Y., Ma, M., Yang, T., Chen, W., Yang, T., 2018. Global atmospheric sulfur deposition and associated impaction on nitrogen cycling in ecosystems. J. Clean. Prod. 195, 1–9.
Geddes, J.A., Martin, R.V., 2017. Global deposition of total reactive nitrogen oxides from 1996 to 2014 constrained with satellite observations of NO_2 columns. Atmos. Chem. Phys. 17, 10071–10091.
Geddes, J.A., Martin, R.V., Boys, B.L., van Donkelaar, A., 2016. Long-term trends worldwide in ambient NO_2 concentrations inferred from satellite observations. Environ. Health Perspect. 124, 281.
Graaf, S.C.v.d., Dammers, E., Schaap, M., Erisman, J.W., 2018. How are NH_3 dry deposition estimates affected by combining the LOTOS-EUROS model with IASI-NH3 satellite observations? Atmos. Chem. Phys. 18, 13173–13196.
Gu, B., Ju, X., Chang, J., Ge, Y., Vitousek, P.M., 2015. Integrated reactive nitrogen budgets and future trends in China. P. Nat. Aca. Sci. USA. 112, 8792–8797.
Gu, B., Sutton, M.A., Chang, S.X., Ge, Y., Chang, J., 2014. Agricultural ammonia emissions contribute to China's urban air pollution. Front. Ecol. Environ. 12, 265–266.
Hasheminassab, S., Daher, N., Saffari, A., Wang, D., Ostro, B., Sioutas, C., 2014. Spatial and temporal variability of sources of ambient fine particulate matter (PM 2.5) in California. Atmos. Chem. Phys. 14, 12085–12097.
Hedeker, D., 2010. A mixed-effects multinomial logistic regression model. Stat. Med. 22, 1433–1446.
Huang, X., Song, Y., Li, M., Li, J., Huo, Q., Cai, X., Zhu, T., Hu, M., Zhang, H., 2012. A high resolution ammonia emission inventory in China. Global Biogeochem. Cycles 26, 1–14.
Kloog, I., Sorek-Hamer, M., Lyapustin, A., Coull, B., Wang, Y., Just, A.C., Schwartz, J., Broday, D.M., 2015. Estimating daily PM 2.5 and PM 10 across the complex geo-climate region of Israel using MAIAC satellite-based AOD data. Atmos. Environ. 122, 409–416.
Lü, C., Tian, H., 2007. Spatial and temporal patterns of nitrogen deposition in China: synthesis of observational data. J. Geophys. Res. Atmos. 112.
Lamsal, L.N., Duncan, B.N., Yoshida, Y., Krotkov, N.A., Pickering, K.E., Streets, D.G., Lu, Z., 2015. U.S. NO_2 trends (2005-2013): EPA air quality system (AQS) data versus improved observations from the Ozone monitoring instrument (OMI). Atmos. Environ. 110, 130–143.
Lamsal, L.N., Martin, R.V., van Donkelaar, A., Celarier, E.A., Bucsela, E.J., Boersma, K.F., Dirksen, R., Luo, C., Wang, Y., 2010. Indirect validation of tropospheric nitrogen dioxide retrieved from the OMI satellite instrument: insight into the seasonal variation of nitrogen oxides at northern midlatitudes. J. Geophys. Res. Atmos. 115, 1–15.
Larssen, T., Lydersen, E., Tang, D., He, Y., Gao, J., Liu, H., Duan, L., Seip, H.M., Vogt, R.D., Mulder, J., Shao, M., Wang, Y., Shang, H., Zhang, X., Solberg, S., Aas, W., Okland, T., Eilertsen, O., Angell, V., Li, Q., Zhao, D., Xiang, R., Xiao, J., Luo, J., 2006. Acid rain in China. Environ. Sci. Technol. 40, 418–425.
Li, Q., Cui, X., Liu, X., Roelcke, M., Pasda, G., Zerulla, W., Wissemeier, A.H., Chen, X., Goulding, K., Zhang, F., 2017a. A new urease-inhibiting formulation decreases ammonia volatilization and improves maize nitrogen utilization in North China Plain. Sci. Rep. 7, 43853.
Li, T., Zhang, W., Yin, J., Chadwick, D., Norse, D., Lu, Y., Liu, X., Chen, X., Zhang, F., Powlson, D., Dou, Z., 2017b. Enhanced-efficiency fertilizers are not a panacea for resolving the nitrogen problem. Global Change Biol. 24, e511–e521.
Li, Y., Schichtel, B.A., Walker, J.T., Schwede, D.B., Chen, X., Lehmann, C.M., Puchalski, M.A., Gay, D.A., Collett, J.L., 2016. Increasing importance of deposition of reduced nitrogen in the United States. P. Nat. Aca. Sci. USA. 113, 5874–5879.
Liu, J., Price, D.T., Chen, J.M., 2005. Nitrogen controls on ecosystem carbon sequestration: a model implementation and application to Saskatchewan, Canada. Ecol. Model. 186, 178–195.
Liu, L., Zhang, X., Wang, S., Lu, X., Ouyang, X., 2016. A review of spatial variation of inorganic nitrogen (N) wet deposition in China. PloS One 11, e0146051.
Liu, L., Zhang, X., Wong, A.Y.H., Xu, W., Liu, X., Li, Y., Mi, H., Lu, X., Zhao, L., Wang, Z., Wu, X., 2019. Estimating global surface ammonia concentrations inferred from satellite retrievals. Atmos. Chem. Phys. 19, 12051–12066.
Liu, L., Zhang, X., Xu, W., Liu, X., Lu, X., Chen, D., Zhang, X., Wang, S., Zhang, W., 2017a. Estimation of monthly bulk nitrate deposition in China based on satellite NO_2 measurement by the Ozone Monitoring Instrument. Remote Sens. Environ. 199, 93–106.
Liu, L., Zhang, X., Xu, W., Liu, X., Lu, X., Wang, S., Zhang, W., Zhao, L., 2017b. Ground ammonia concentrations over China derived from satellite and atmospheric transport modeling. Rem. Sens. 9, 467.
Liu, L., Zhang, X., Zhang, Y., Xu, W., Liu, X., Zhang, X., Feng, J., Chen, X., Zhang, Y., Lu, X., Wang, S., Zhang, W., Zhao, L., 2017c. Dry particulate nitrate deposition in China. Environ. Sci. Technol. 51, 5572–5581.
Liu, X., Duan, L., Mo, J., Du, E., Shen, J., Lu, X., Zhang, Y., Zhou, X., He, C., Zhang, F., 2011. Nitrogen deposition and its ecological impact in China: an overview. Environ. Pollut. 159, 2251–2264.
Liu, X., Vitousek, P., Chang, Y., Zhang, W., Matson, P., Zhang, F., 2015. Evidence for a historic change occurring in China. Environ. Sci. Technol. 50, 505–506.
Liu, X., Zhang, Y., Han, W., Tang, A., Shen, J., Cui, Z., Vitousek, P., Erisman, J.W., Goulding, K., Christie, P., 2013. Enhanced nitrogen deposition over China. Nature 494, 459–462.
Mentel, T.F., Bleilebens, D., Wahner, A., 1996. A study of nighttime nitrogen oxide oxidation in a large reaction chamber—the fate of NO2, N2O5, HNO3, and O3 at different humidities. Atmos. Environ. 30, 4007–4020.
Miyazaki, K., Eskes, H., Sudo, K., Takigawa, M., van Weele, M., Boersma, K., 2012. Simultaneous assimilation of satellite NO2, O3, CO, and HNO3 data for the analysis of tropospheric chemical composition and emissions. Atmos. Chem. Phys. 12, 9545–9579.
Morrell, C.H., 1998. Likelihood ratio testing of variance components in the linear mixed-effects model using restricted maximum likelihood. Biometrics 54, 1560–1568.
Pan, Y., Wang, Y., Tang, G., Wu, D., 2012. Wet and dry deposition of atmospheric nitrogen at ten sites in Northern China. Atmos. Chem. Phys. 12, 6515–6535.
Piao, S., Ciais, P., Huang, Y., Shen, Z., Peng, S., Li, J., Zhou, L., Liu, H., Ma, Y., Ding, Y., Friedlingstein, P., Liu, C., Tan, K., Yu, Y., Zhang, T., Fang, J., 2010. The impacts of climate change on water resources and agriculture in China. Nature 467, 43.
Schaub, D., Boersma, K., Kaiser, J., Weiss, A., Folini, D., Eskes, H., Buchmann, B., 2006. Comparison of GOME tropospheric NO 2 columns with NO 2 profiles deduced from ground-based in situ measurements. Atmos. Chem. Phys. 6, 3211–3229.
Skiba, U., Dick, J., Storetonwest, R., Fernadeslopez, S., 2006. The relationship between ammonia emissions from a poultry farm and soil NO and N2O fluxes from a downwind source. Biogeosci. Discuss. 2, 977–995.
Sportisse, B., 2007. A review of parameterizations for modelling dry deposition and scavenging of radionuclides. Atmos. Environ. 41, 2683–2698.
Stram, D.O., 1996. Meta-analysis of published data using a linear mixed-effects model. Biometrics 52, 536–544.
Sutton, M.A., Reis, S., Riddick, S.N., Dragosits, U., Nemitz, E., Theobald, M.R., Tang, Y.S., Braban, C.F., Vieno, M., Dore, A.J., Mitchell, R.F., Wanless, S., Daunt, F., Fowler, D., Blackall, T.D., Milford, C., Flechard, C.R., Loubet, B., Massad, R., Cellier, P., Personne, E., Coheur, P.F., Clarisse, L., Van Damme, M., Ngadi, Y., Clerbaux, C., Skjøth, C.A., Geels, C., Hertel, O., Wichink Kruit, R.J., Pinder, R.W., Bash, J.O., Walker, J.T., Simpson, D., Horváth, L., Misselbrook, T.H., Bleeker, A., Dentener, F., de Vries, W., 2013. Towards a climate-dependent paradigm of ammonia emission and deposition. Phil. Trans. Biol. Sci. 368.
Sutton, M.A., Tang, Y.S., Miners, B., Fowler, D., 2001. A new diffusion denuder system for long-term, regional monitoring of atmospheric ammonia and ammonium. Water Air Soil Pollut. Focus 1, 145–156.
Tørseth, K., Aas, W., Breivik, K., Fjæraa, A.M., Fiebig, M., Hjellbrekke, A.G., Lund Myhre, C., Solberg, S., Yttri, K.E., 2012. Introduction to the European Monitoring and Evaluation Programme (EMEP) and observed atmospheric composition change during 1972-2009. Atmos. Chem. Phys. 12, 5447–5481.
Tan, J., Fu, J.S., Dentener, F., Sun, J., Emmons, L., Tilmes, S., Sudo, K., Flemming, J., Jonson, J.E., Gravel, S., 2018. Multi-model study of HTAP II on sulfur and nitrogen deposition. Atmos. Chem. Phys. 18, 1–36.
Van Damme, M., Clarisse, L., Dammers, E., Liu, X., Nowak, J., Clerbaux, C., Flechard, C., Galy-Lacaux, C., Xu, W., Neuman, J., 2014. Towards validation of ammonia (NH_3) measurements from the IASI satellite. Atmos. Meas. Tech. 7, 12125–12172.
Van Damme, M., Clarisse, L., Whitburn, S., Hadji-Lazaro, J., Hurtmans, D., Clerbaux, C., Coheur, P.-F., 2018. Industrial and agricultural ammonia point sources exposed. Nature 564, 99–103.
Van Damme, M., Whitburn, S., Clarisse, L., Clerbaux, C., Hurtmans, D., Coheur, P.F., 2017. Version2 of the IASI NH_3 neural network retrieval algorithm: near-real-time and reanalysed datasets. Atmos. Meas. Tech. 10, 1–14.
Wang, S., Zhang, Q., Streets, D., He, K., Martin, R., Lamsal, L., Chen, D., Lei, Y., Lu, Z., 2012. Growth in NO_x emissions from power plants in China: bottom-up estimates and satellite observations. Atmos. Chem. Phys. 12, 4429–4447.
Warner, J.X., Dickerson, R.R., Wei, Z., Strow, L.L., Wang, Y., Liang, Q., 2017. Increased atmospheric ammonia over the world's major agricultural areas detected from space. Geophys. Res. Lett. 44, 2875–2884.
Wei, Jing, Zhanqing Li, Maureen Cribb, Wei Huang, Wenhao Xue, Lin Sun, Jianping Guo, Yiran Peng, Jing Li, Alexei Lyapustin, Lei Liu, Hao Wu, and Yimeng Song, 2020. Improved 1 km resolution $PM_{2.5}$ estimates across China using enhanced space–time extremely randomized trees. Atmospheric Chemistry and Physics 20, 3273–3289. https://doi.org/10.5194/acp-20-3273-2020.
Wei, J., Huang, W., Li, Z., Xue, W., Peng, Y., Sun, L., Cribb, M., 2019a. Estimating 1-km-resolution PM2.5 concentrations across China using the space-time random forest approach. Remote Sens. Environ. 231, 111221.
Wei, J., Li, Z., Guo, J., Sun, L., Huang, W., Xue, W., Fan, T., Cribb, M., 2019b. Satellite-derived 1-km-Resolution PM1 concentrations from 2014 to 2018 across China. Environ. Sci. Technol. 53, 13265–13274.
Wesely, M., Hicks, B., 1977. Some factors that affect the deposition rates of sulfur dioxide and similar gases on vegetation. J. Air Pollut. Contr. Assoc. 27, 1110–1116.
Xu, W., Liu, L., Cheng, M., Zhao, Y., Zhang, L., Pan, Y., Zhang, X., Gu, B., Li, Y., Zhang, X., Shen, J., Lu, L., Luo, X., Zhao, Y., Feng, Z., Collett Jr., J.L., Zhang, F., Liu, X., 2018. Spatial-temporal patterns of inorganic nitrogen air concentrations and deposition in eastern China. Atmos. Chem. Phys. 18, 10931–10954.
Xu, W., Luo, X.S., Pan, Y.P., Zhang, L., Tang, A.H., Shen, J.L., Zhang, Y., Li, K.H., Wu, Q.H., Yang, D.W., Zhang, Y.Y., Xue, J., Li, W.Q., Li, Q.Q., Tang, L., Lv, S.H., Liang, T., Tong, Y.A., Liu, P., Zhang, Q., Xiong, Z.Q., Shi, X.J., Wu, L.H., Shi, W.Q., Tian, K., Zhong, X.H., Shi, K., Tang, Q.Y., Zhang, L.J., Huang, J.L., He, C.E., Kuang, F.H., Zhu, B., Liu, H., Jin, X., Xin, Y.J., SHi, X.K., Du, E.Z., Dore, A.J., Tang, S., Collett Jr., J.L., Goulding, K., Sun, Y.X., Ren, J., Zhang, F.S., Liu, X.J., 2015. Quantifying atmospheric nitrogen deposition through a nationwide monitoring network across China. Atmos. Chem. Phys. 15, 12345–12360.
Xu, W., Zhang, L., Liu, X., 2019. A database of atmospheric nitrogen concentration and deposition from the nationwide monitoring network in China. Sci. Data 6, 51.

Yap, X., Hashim, M., 2013. A robust calibration approach for PM10 prediction from MODIS aerosol optical depth. Atmos. Chem. Phys. 13, 3517–3526.
Yu, G., Jia, Y., He, N., Zhu, J., Chen, Z., Wang, Q., Piao, S., Liu, X., He, H., Guo, X., Wen, Z., Li, P., Ding, G., Goulding, K., 2019. Stabilization of atmospheric nitrogen deposition in China over the past decade. Nat. Geosci. 12, 424–429.
Zhang, L., Wright, L.P., Asman, W.A.H., 2010. Bi-directional air-surface exchange of atmospheric ammonia: a review of measurements and a development of a big-leaf model for applications in regional-scale air-quality models. J. Geophys. Res. Atmos. 115, 898–907.
Zhang, X., Wu, Y., Liu, X., Reis, S., Jin, J., Dragosits, U., Van Damme, M., Clarisse, L., Whitburn, S., Coheur, P.-F., Gu, B., 2017a. Ammonia emissions may Be substantially underestimated in China. Environ. Sci. Technol. 51, 12089–12096.
Zhang, X., Zhang, Y., Fath, B.D., 2020. Analysis of anthropogenic nitrogen and its influencing factors in Beijing. J. Clean. Prod. 244, 118780.
Zhang, X.Y., Lu, X.H., Liu, L., Chen, D.M., Zhang, X.M., Liu, X.J., Zhang, Y., 2017b. Dry deposition of NO_2 over China inferred from OMI columnar NO_2 and atmospheric chemistry transport model. Atmos. Environ. 169.
Zhang, Y., Mathur, R., Bash, J.O., Hogrefe, C., Xing, J., Roselle, S.J., 2018. Long-term trends in total inorganic nitrogen and sulfur deposition in the U.S. from 1990 to 2010. Atmos. Chem. Phys. 1–27.
Zhao, X., Chen, L., Zhang, H., 2013. Nitrate and ammonia contaminations in drinking water and the affecting factors in Hailun, northeast China. J. Environ. Health 75, 28.
Zhao, Y., Zhang, L., Chen, Y., Liu, X., Xu, W., Pan, Y., Duan, L., 2017. Atmospheric nitrogen deposition to China: a model analysis on nitrogen budget and critical load exceedance. Atmos. Environ. 153, 32–40.
Zhu, J., He, N., Wang, Q., Yuan, G., Wen, D., Yu, G., Jia, Y., 2015. The composition, spatial patterns, and influencing factors of atmospheric wet nitrogen deposition in Chinese terrestrial ecosystems. Sci. Total Environ. 511, 777–785.